DEUTSCHES ELEKTRONEN-SYNCHROTRON DESY

DESY SR-79/29
November 1979

X-RAY SOURCES

by

U. Bonse
Institut für Physik der Universität Dortmund

NOTKESTRASSE 85 · 2 HAMBURG 52

To be sure that your preprints are promptly included in the
HIGH ENERGY PHYSICS INDEX ,
send them to the following address (if possible by air mail) :

DESY
Bibliothek
Notkestrasse 85
2 Hamburg 52
Germany

DESY SR-79/29
November 1979

X-ray sources *

U. Bonse

Institut für Physik, University of Dortmund, Fed. Rep. of Germany

1. DEFINITION OF A 'POWERFUL' SOURCE

The development of more powerful sources plays a major role in the overall improvement of X-ray techniques in general and of topography in particular. In recent years some progress has been made to increase the brightness and also the total photon flux of conventional sealed off X-ray tubes. Rotating anode tubes have been developed to greater variety, to more reliability and to higher brightness and flux. Synchrotron radiation has entered the field of X-ray diffraction and, with the increasing availability of storage rings dedicated to the production of synchrotron X-rays, will presumably replace conventional X-ray sources in many experiments in the near future. Compared with a conventional source a synchrotron source is rather costy and, in general, requires the individual experimenter to leave his home laboratory, transfer his equipment to the synchrotron radiation center and start using X-rays as member of a 'users community' at the storage ring. Considering the amount of financial and organisational disadvantages experienced by the newcomer to the big facility it is very important to find out clearly whether the synchrotron source is better for the particular problem to be solved and how much it is better. With this respect the statement, the synchrotron source is 'more intense' is certainly not adequate, since, with this generality, it may not even be true in the particular case. Hence it is highly desirable to define the powerfulness of a source precisely.

Certainly a 'better' (more powerful) source is one which delivers a larger number of photons per time interval to the detecting

* to be published in Plenum Press as Proceedings of the Nato Advanced Study Institute "The characterization of crystal defects by x-ray methods", Durham, 1979

system of a particular experiment under otherwise equal parameters of geometry and resolution, where resolution refers to spacial, angular, spectral and/or time resolution depending whatever the method is specifically aiming at. From this definition of powerfulness it is obvious that it cannot be given for the source alone but that the acceptance and transmittance properties of the measuring apparatus have to be included.

For a quantitative discussion we define the following source characteristics (Fig. 1):

brightness $n(x, z, \xi, \psi, E, t)$ [phot. s^{-1} mm^{-2} $mrad^{-2}$ per 0.1% $\Delta E/E$], gives the number of photons emitted at time t from the source point (x, z) along the direction (ξ, ψ) with energy E per time interval, unit source area, unit solid angle and 0.1% bandwidth

intensity $N(\xi, \psi, E, t) \equiv \int_{\text{source}} n\, dx dz$ [phot. s^{-1} $mrad^{-2}$ per 0.1% $\Delta E/E$]

partially integrated intensity

$$N'(\xi, E, t) \equiv \int_{-\tau/2}^{+\tau/2} N d\psi \quad [\text{phot. } s^{-1} \text{ mrad}^{-1} \text{ per } 0.1\% \ \Delta E/E]$$

With a synchrotron radiation source the integration is normal to the plane of the electron orbit.

spectral flux $\Phi_S(E, t) = \int_{\Omega} N d\xi d\psi$ [phot. s^{-1} per 0.1% $\Delta E/E$]

Ω is solid angle of beam.

total flux $\Phi_T(t) = 10^3 \int_{>0}^{\infty} E^{-1} \Phi_S dE$ [phot. s^{-1}]

σ_x, σ_z [mm] is standard deviation of horizontal, vertical source or beam size, respectively. Source area $A \equiv \sigma_x \sigma_y (2.35)^2$ [mm^2] (Full width at half maximum is 2.35σ)

σ'_x, σ'_z [mrad] is standard deviation of horizontal, vertical beam divergence respectively. $\Omega = \sigma'_x \cdot \sigma'_y (2.35)^2$

horizontal emittance $\varepsilon_x \equiv \sigma_x \sigma'_x$ [mm mrad]

vertical emittance $\varepsilon_z \equiv \sigma_z \sigma'_z$ [mm mrad]

The parameters defined above can be marked with subscripts σ and π if σ- and π-polarization states have to be distinguished. It should be noted that n, N, N', Φ_S and Φ_T give number of photons per sec and not directly radiated power.

For a source to be 'powerful' or to be better than another source, different techniques usually require different source parameters to be maximized. We shall illustrate the situation by giving a few examples:

(a) Fluorescent spectroscopy: Φ_T should be large over a certain energy range. The values of n, N, A and to some extent also of Ω are not important.

(b) Focusing X-ray optics, techniques employing narrow slit systems and topographic techniques, where the geometrical resolution depends on the source size: n should be large.

(c) Perfect crystal techniques: N should be large and σ'_z equal to or smaller than the perfect crystal diffraction range. n needs not necessarily be large since mostly relatively wide beams can be used.

(d) Time resolved studies: a sharp pulse structure of n, N, Φ_S and Φ_T is advantageous.

We shall see below that with respect to the above requirements synchrotron sources and conventional X-ray tubes can score with different techniques totally different.

In general, X-rays can be produced in at least three principially different ways: by electron impact on (usually) solid targets (EI), by fluorescent excitation (FE) and as synchrotron radiation (SR) from electrons or positrons orbiting in synchrotrons and storage rings or following curved paths in special magnet systems like wigglers and undulators set up at storage rings. Due to their generally low intensity, FE sources play no role in topography, and we shall not discuss them further.

2. X-RAYS GENERATED BY ELECTRON IMPACT ON SOLID TARGETS (EI)

The most common method to produce X-rays is to employ an X-ray tube. Electrons emitted from a hot tungsten wire (cathode) are accelerated towards the target (anode) by applying a suitable DC voltage from 10 kV to 100 kV between cathode and anode. In rare cases in which extremely hard X-rays are wanted a betatron operated in the MeV range [1, 2] can be employed for electron acceleration. For X-ray diffraction topography X-ray energies above 100 keV are practically not needed.

As is well known, the spectrum obtained with EI consists of two parts: the continous bremsspectrum and the spectrum determined by the atomic level system of the element(s) composing the target.

2.1. Bremsspectrum

For the thick targets which have to be used in high power tubes, it is practically impossible to calculate precisely the characteristics of the continuum radiation like polarization, spectral and space distribution. In order to estimate

the intensity for a comparison with SR sources we use the approximate expression which was derived by Kulenkampff and coworkers [3, 4, 5] from experimental data

$$I_\nu = Cz\ (\nu_o - \nu) \quad [\text{erg s}] \qquad (1)$$

where I_ν is the energy radiated by one electron at frequency ν per unit frequency into 4 π solid angle. z is the atomic number of the target material and $\nu_o = E_e/h$ the upper frequency limit as determined by the electron energy $E_e = eU$. U is the tube voltage, e the electron charge and h Planck's constant.

$$C = (5 \pm 1.5) \times 10^{-50} \quad [\text{erg s}^2]$$

is an empirically found constant.

The actual continuum spectrum differs from that given by equation (1) mainly due to absorption in the target. The effect is considerable at the high energy side of the absorption edge(s) of the target material and varies also with the take off angle δ of the X-ray beam. Nevertheless the total intensity is fairly well given by integration of I_ν over ν. We set $E = h\nu$ the photon energy normalize to an energy band $\Delta E/E = \Delta\nu/\nu = \Delta\lambda/\lambda = 10^{-3}$ and obtain per electron and 4 π solid angle

$$I_{0.1\%} \simeq 10^{-3}\ C\ \frac{z}{h^2}\ E_e E\ \left(1 - \frac{E}{E_e}\right) \quad [\text{erg}] \qquad (2)$$

From (2) we calculate the spectral flux Φ_{SB} generated by a current i [mA] (i.e. i x 6.24 x 10^{15} electrons s^{-1}) with $C = 5.75 \times 10^{-50}$ erg s^2

$$\Phi_{SB}(E) \simeq 1.3 \times 10^{7}\ zUi\ \left(1 - \frac{E}{Ue}\right) [\text{phot.s}^{-1} \text{ per } 0.1\%\ \frac{\Delta E}{E}] \qquad (3)$$

where U is in kV and E in keV.

It should be noted, that in the low energy limit (long wavelength) the number Φ_{SB} of bremsstrahlung photons per 10^{-3} bandwidth becomes independent of E.

We shall use (3) to make a rough estimate of the number N_B of bremsstrahlung photons diffracted by a perfect crystal in a typical topography experiment. Let the source (Fig. 1) and the slit have a size of $\sigma_x \cdot \sigma_z$ = 5 mm x 0.5 mm each and be 10^3 mm apart. Then $\sigma_z' = 1$ mrad and with an assumed Bragg angle $\Theta_B = 45^o$ we have $\sigma_z' = \Delta\lambda/\lambda = \Delta E/E = 10^{-3}$. Thus the energy band is of the order assumed in deriving equation (3). However, for a fixed λ and hence fixed E the accepted divergence is determined by the perfect crystal diffraction range $\Delta\Theta_p = 0.1$ mrad which is considerably less than σ_z'. Furthermore $\sigma_x' = 10$ mrad, hence the solid angle accepted by the crystal at fixed E is $\Delta\Omega = \sigma_x' \Delta\Theta_p = 1$ mrad^2 i.e. N_B is in effect the source intensity N defined at the beginning. It follows

$$N_B = Ui z\left(1 - \frac{E}{U_e}\right) [\text{phot.s}^{-1} \text{ mrad}^{-2} \text{ per } 0.1\%\ \frac{\Delta E}{E}] \qquad (4)$$

Values of N_B for U = 40 kV, i = 40 mA are given in Table 1 for typical target materials at their corresponding K_α-energies for comparison with estimates of characteristic line intensities (section 2.2). It may be noted that for photographic exposure these intensities are extremely low. As will be shown, with characteristic lines and with SR much higher intensities can be obtained.

The bremsstrahlung is found to be slightly polarized parallel (i.e. π) to the direction of the electron beam [6, 7]. Very close to the short wavelength limit the polarization P is largest, where as usual we define

$$P \equiv \frac{N_{\pi} - N_{\sigma}}{N_{\pi} + N_{\sigma}} \qquad (5)$$

Values of P between 10% [6] and 46% [7] have been observed. Observations on Pt, Ag, Cu and Fe targets failed to reveal any significant dependence of polarization on atomic number.

With thick targets, the variation of emitted intensity with angle is not very pronounced. Nevertheless there is a maximum of emission at right angles to the incident electron beam (if the detection is not impossible because of absorption). With increasing voltage the maximum shifts somewhat towards the direction of the electron beam [8].

2.2. Characteristic line spectrum

The question of how many characteristic X-rays will be generated when one electron hits the target was studied by Green [9] who measured line intensities for a number of target elements at different tube voltages U and compared them with the theory by Green and Cosslett [10]. Satisfactory agreement of experiment and theory was observed for the K-series but not for the L-series. According to Green's experimental results, the total number P_j of quanta generated per electron in a line j (j = K_α, K_β, L_α, etc.) is

$$P_j = K_{jz} \, (E_e - E_{ejz})^{1.63} \qquad (6)$$

E_e is the electron energy and E_{ejz} is the minimum excitation energy in keV for the element with atomic number z and the series to which the line j belongs. Values of E_{ejz} as well as of E_{jz}, the energies of characteristic lines, are tabulated in [11]. K_{jz} are experimental quantum efficiencies of characteristic X-ray

production given in [9]. For a particular line j, K_{jz} depends on z but not on the tube voltage U. From the data given in [9] we have derived K_{jz} values for some common target materials (Table 2). Observed is not directly P_j but rather P_j f (δ)/4 π, where $P_j/4\pi$ is the number of quanta generated by one electron per steradian. f (δ) is a factor taking into account the absorption within the target. f (δ) depends on U, on the take off angle δ between X-ray beam and surface and on the incidence angle of the electron beam. Green [12] measured f (δ) at normal incidence for the K_α lines of C, Al, Ti, Fe, Cu, Ge, Mo and Ag and for the $L_{\alpha 1}$ lines of Nd, Ta and Au. Values taken from [12] for $\delta = 6^\circ$, the usual take off angle with X-ray tubes, and for different tube voltage are given in Table 2.

For the comparison with the continous spectrum (equation (4)) we derive the observable intensity N_L of characteristic lines per mrad^2 generated by a current i [mA]

$$N_L \approx 5 \times 10^8 \, K_{jz} \, f(\delta) \, i \, (E_e - E_{jz})^{1.63} \left[\text{phot.s}^{-1}\text{mrad}^{-2} \text{ per } 0.1\% \, \frac{\Delta E}{E}\right] \qquad (7)$$

where E_e and E_{jz} are in keV. Values of N_L calculated for U = 40 kV, i = 40 mA, $\delta = 6^\circ$ are given in Table 1 for five different lines. When comparing N_L with corresponding intensities N_B of the continuum is has to be remembered that the bandwidth $\Delta E/E \approx 3$ to 5×10^{-4} for characteristic lines (natural line width of Mo $K_{\alpha 1}$ (Mo $K_{\alpha 2}$) is 3.79×10^{-4} (3.93×10^{-4}), respectively [13]) whereas N_B is normalized to $\Delta E/E = 10^{-3}$. This means that N_B is in effect even about 1/3 to 1/2 lower when normalized to the same bandwidth. Furthermore, the same solid angle $\Delta\Omega = 1$ mrad^2 can be realized with a diffracting perfect crystal by making $\sigma'_x = 10$ mrad as before. Again for a fixed λ, $\sigma'_z = \Delta\Theta_p \approx 10^{-1}$ mrad is determined by the perfect crystal diffraction range $\Delta\Theta_p$, hence $\Delta\Omega = 1$ mrad^{-2}. As is seen by comparison of N_L and N_B of Table 1,

the line intensities are roughly 10^3 times larger than the corresponding bremsstrahlung intensities.

Regarding the relative intensities of different lines of the same series the following empiric rules hold [13]

(a) for most elements $N_{K\alpha 1} = 2\ N_{K\alpha 2}$

(b) $N_{K\alpha 1} : N_{K\alpha 2} : N_{K\beta 2} \approx \begin{cases} 100 : 50 : 35 \text{ for W} \\ 100 : 50 : 25 \text{ for Cu} \end{cases}$

2.3. Efficiency of X-ray production by EI

The total intensity I_T per incident electron contained in the continous spectrum is obtained by integrating equation (1)

$$I_T = \int_0^{\nu_o} I_\nu \, d_\nu = \frac{1}{2} C \, z \, \frac{e^2 U^2}{h^2} \qquad (8)$$

Dividing by eU, the energy applied by the impinging electron we obtain the efficiency η_B for bremsstrahlung generation

$$\eta_B = \frac{1}{2} C z \frac{eU}{h^2} \approx 10^{-6} \, zU \qquad (9)$$

where U is in kV. Equation (9) is in agreement with measurements and calculations by Rump [14], Kramers [15] and Kulenkampff and Schmidt [5]. With z = 42 (Mo) and U = 40 kV we have $\eta_B \approx 1.7 \times 10^{-3}$ which is very low.

The energy of the characteristic radiation per incident electron is calculated by multiplying equation (6) with E_{jz}, the quantum energy of the emitted radiation

$$I_L = K_{jz} E_{jz} (E_e - E_{ejz})^{1.63} \qquad (10)$$

Dividing again by $eU = E_e$, the energy applied by the incident electron, we obtain the efficiency η_L for the generation of characteristic radiation

$$\eta_L = \frac{K_{jz}}{eU} E_{jz} (eU - E_{ejz})^{1.63} \qquad (11)$$

For a typical line like Mo Kα with E_{jz} = 17.5 keV, E_{ejz} = 20 keV, $K_{jz} = 6.4 \times 10^{-6}$ (Table 2) generated with a tube voltage of U = 40 kV we calculate $\eta_L = 3.7 \times 10^{-4}$ which is even lower than η_B.

It follows, that practically the total energy of the electron beam is converted into heat. Thus the problem of anode cooling sets in effect the limit to the total flux Φ_T of an X-ray tube.

2.4 X-ray tubes

There are two principal objectives in designing an X-ray tube: first to cool away as much power as possible in order to obtain a high total flux Φ_T and, secondly, to keep the size of the focus small in order to increase the brightness n, which, as is known from general principles cannot be increased by optical instruments. Since the maximum specific load, i.e. the dissipated power per focal area, increases with decreasing focus size, Φ_T and n cannot be optimized simultaneously. Consequently it depends on the major intended use of the tube whether the design favours Φ_T (spectroscopy tube) or n (fine focus diffraction tube). A certain flexibility is achieved when the focal size can be changed by focusing the electron beam on the anode more or less. However, focusing electron guns require to apply to the Wehnelt cylinder (Fig. 2) an adjustable potential close to the cathode potential which usually is at high potential against ground. Hence the provision of a focussing potential complicates the design of the high voltage generator and is thus available with more expensive units only.

The specific load can be increased considerably by placing the focus always on a fresh, cooled face, i.e. by moving the anode away under a stationary focused electron beam. The technical solution to this idea are X-ray generators with rotating anode tubes. A sealed off tube with stationary anode is illustrated by Fig. 2. Fig. 3 shows the principal construction features of a pumped tube with a water cooled rotating anode.

It is obvious that the operation of sealed off tubes is very much simpler than that of rotating anode tubes, where the coolant has to be supplied through a rotating shaft and all the means of making and controlling an excellent vacuum are needed. Nevertheless, because of the considerable gain in Φ_T and/or n, there are a number of powerful rotating anode generators on the market. An excellent description of rotating anode tubes which includes also aspects of design has recently been given by Yoshimatsu and Kozaki [16].

We give a survey of presently available tubes by listing in Table 3 their main parameters like focus size, maximum load and maximum specific load, brightness n_B and n_L and intensities N_B, N_L for bremsstrahlung and characteristic radiation respectively. n_B, n_L, N_B and N_L are given for E = 17.5 keV (Mo Kα-radiation) and take off angle $\delta = 6^o$ with the tube operated at $U = U_{max}$ and maximum total load. The data are specifically useful for the comparison with SR sources (Table 5).

3 SYNCHROTRON X-RAY SOURCES

3.1 General

As is well known, charged particles orbiting in circular accelerators emit synchrotron radiation (SR). The total emitted intensity is proportional [17] to γ^4 where

$$\gamma = \frac{E_e}{mc^2} \qquad (12)$$

E_e is the particle energy and m the particle mass. It follows from equation (12) that, for a given energy E_e, SR from light

particles like electrons and positrons is much more intense than that from heavier particles like protrons etc. SR has a continous spectrum with a maximum which shifts to shorter wavelengths proportional to E_e^{-3}. Over the last decade, E_e in electron (positron) accelerators increased more and more. As a consequence SR also in the X-ray region below 10 Å wavelength became available.

For diffraction topography SR was first used in 1973 by Tuomi, Naukkarinen, Laurila and Rabe [18, 19], who made topographs of a silicon crystal with SR from DESY. Hart [20] obtained topographs of silicon and lithiumfluoride crystals with SR from NINA. Early uses of SR X-rays included X-ray interferometry [21], EXAFS measurements [22], small angle scattering [23] and photoelectronspectroscopy (XPS) [24]. Since then it became more and more apparent that, because of the unique properties of SR, namely continous spectrum, high Φ_s, N and n, extreme collimation, sharp time structure and defined polarization states, SR is not only very well suited for diffraction topography and other known X-ray techniques but may open up entirely new experimental possibilities in the X-ray range. A survey of X-ray investigations performed with SR may be found in the last section of the article by Gudat and Kunz [25]. In Table 5 we give a list of twelve storage rings which, as far as their machine parameters are concerned, are in principle capable of generating SR in the X-ray range. Except the European Synchrotron Radiation Facility (ESRF), for which there is only a study report so far [26], all other rings are either in operation, under construction or in the planning stage.

That up to now so little SR topography has been employed is mainly due to the limited availability of synchrotron X-rays in the past. The situation no doubt will change when more storage rings exist for SR dedicated operation in the X-ray region.

3.2 Calculation of the radiation properties of a SR source

The radiation properties of a SR source can be calculated from exact analytical expressions, which, as we have seen, is impossible with EI X-ray sources. Thus a further advantage of SR is that it can be used for calibration purposes over a wide range of wavelengths [27, 28, 29].

We briefly summarize the theoretical expressions describing SR. Further details may be found in reviews in the literature [30, 31, 32].

The instantaneous power I (λ, ψ) radiated by a monoenergetic electron along a circular orbit per unit wavelength and radian of angle ψ against the orbital plane is [33] (Fig. 4)

$$I(\lambda, \psi) = \frac{27}{32\pi^3} \frac{e^2 c}{R^3} \left(\frac{\lambda_c}{\lambda}\right)^4 \gamma^8 \left[1 + (\gamma\psi)^2\right]^2 \cdot \left\{ K_{2/3}^2(\xi) + \frac{(\gamma\psi)^2}{1 + (\gamma\psi)^2} K_{1/3}^2(\xi) \right\} \tag{13}$$

R is the radius of the orbit. λ_c is the so called 'critical wavelength' given by

$$\lambda_c \equiv \frac{4\pi R}{3} \gamma^{-3} \tag{14}$$

or

$$\lambda_c\,[\text{Å}] = 5.59R\,[\text{m}]\, E_e^{-3}\,[\text{GeV}] = 12.4/E_c[\text{keV}] \tag{15}$$

$K_{2/3}$ and $K_{1/3}$ are modified Bessel functions of the second kind with argument ξ defined by

$$\xi \equiv \frac{\lambda_c}{2\lambda} \left[1 + (\gamma\psi)^2\right]^{3/2} \tag{16}$$

SR is elliptically polarized and the terms

$$K_\pi \equiv K_{2/3}^2(\xi), \quad K_\sigma \equiv \frac{(\gamma\psi)^2}{1 + (\gamma\psi)^2} K_{1/3}(\xi) \tag{17}$$

correspond to the components which are polarized parallel π and perpendicular to the electron orbit. The polarization is

$$p \equiv \frac{I_\pi - I_\sigma}{I_\pi + I_\sigma} = \frac{K_\pi - K_\sigma}{K_\pi + K_\sigma} \tag{18}$$

For all λ SR is completely polarized in the plane of the orbit. The dependence of the two components on ψ for an arbitrary pair λ, E_e is qualitatively shown in Fig. 5. As is seen, I_π is largest for $\psi = 0$, whereas I_σ has its maximum value at a certain angle $\psi_{\sigma m}$ above and below the orbit plane. The total power I (ψ) radiated at elevation angle ψ is obtained by integrating equation (13) over λ [33]

$$I(\psi) = \frac{7}{16} \frac{e^2 c}{R^2} \gamma^5 \left[1 + (\gamma\psi)^2\right]^{-5/2} \left\{ 1 + \frac{5}{7} \frac{(\gamma\psi)^2}{1 + (\gamma\psi)^2} \right\} \tag{19}$$

where again the first term in the big bracket corresponds to parallel and the last term to perpendicular polarization. From (19) one calculates that the intensity of the parallel component falls to one half within a cone of $1.13\,\gamma^{-1}$ opening angle e.g. with E_e = 5 GeV = 0.1 mrad. Similarly one finds the perpendicular component to have maximum intensity at $\psi_{\sigma max} = 0.63\,\gamma^{-1}$. Short wavelengths are even more collimated than the above values which apply to the λ-integrated distribution [30].

The spectral distribution I (λ) of SR is obtained by integrating equation (13) over ψ [34]

$$I(\lambda) = \frac{3^{5/2}}{16\pi^2}\frac{e^2 c}{R^3}\gamma^7\left(\frac{\lambda_c}{\lambda}\right)^3 \int_{\lambda_c/\lambda}^{\infty} K_{5/3}(\eta)\, d\eta \qquad (20)$$

From (20) we obtain $N'(\lambda)$ for a current i [mA] and an X-ray beam of 1 mrad divergence in the y, x-plane (Fig. 4)

$$N'(\lambda) = 7.87\times10^{8}\lambda^2\, i\, \frac{E_e^7}{R^2}\left(\frac{\lambda_c}{\lambda}\right)^3 \int_{\lambda_c/\lambda}^{\infty} K_{5/3}(\eta)\, d\eta \left[s^{-1}\ \text{mrad}^{-1}\ 0.1\%\ \frac{\Delta E}{E}\right] \qquad (21)$$

E_e is in GeV, R in m and λ in Å. We have calculated the distribution $N'(\lambda)$ of equation (21) for the 12 storage rings mentioned above. The results are shown in Fig. 6 together with a list of operational data for which the calculations have been made. In Fig. 6, the energies of typical X-ray lines, namely FeKα (6.40 keV, 1.936 Å), CuKα (8.05 keV, 1.54 Å), MoKα (17.5 keV, 0.71 Å) and AgKα (22.2 keV, 0.56 Å) have been indicated, and the corresponding SR intensites N' are numerically given in Table 5. As mentioned in the beginning, N' is obtained by integration of N with respect to ψ (Fig. 1 and Fig. 4) over the range of the order of σ_z' of vertical divergence. σ_z' as function of the wavelength can be estimated [35] according to

$$\sigma_z' = \frac{0.511}{E_e}\left(\frac{\lambda}{\lambda_c}\right)^{1/3} \qquad \text{for } \lambda \gg \lambda_c \qquad (22)$$

$$\sigma_z' = \frac{0.295}{E_e}\left(\frac{\lambda}{\lambda_c}\right)^{1/2} \qquad \text{for } \lambda \ll \lambda_c \qquad (23)$$

with E_c in GeV. σ_z' is defined as the angular range outside which the intensity has fallen below e^{-1} of the peak at $\psi = 0$. Values of σ_z' at E = 10 keV (λ=1.24 Å) calculated for the 12 storage rings are also listed in Table 5. In all cases $\sigma_z' < 0.1$ mrad which implies, that

the intensities N' are available within the very small solid angle $\Delta\Omega = \sigma_z'\sigma_x' < 0.1\ \text{mrad}\times 1\ \text{mrad} = 0.1\ \text{mrad}^2$. This means that in the orbit plane of SR sources N is more than ten times larger than the N' intensities given in Table 5. However, above and below this plane N falls off rapidly. Both facts have to be remembered, when we compare N' of the SR sources with N_B, N_L of the X-ray tubes as given in Table 3 and Table 4.

3.3 Time structure of SR from storage rings.

In a storage ring only discrete stable positions occur around the orbit with a separation determined by the microwave frequency. A pulse structure with intervals t_p of the order of ns results if all these pockets (some 100 to 500) are filled with electron bunches. The pulse length t_b is 30 to 200 ps. If only one bunch is in the ring the repetition time t_p is about one to five microseconds. For time decay studies or live topography it may be desireable to have t_b as short and t_p as long as possible, e.g. t_b = 30 ps and t_p = 2μs. Live topography requires the intensity within one or a few bunches to be large enough to give a single picture. On the other hand, when the variations of the structure to be investigated can be controlled at will, e.g. by varying a magnetic field or similar, then a stroboscopic imaging technique becomes possible by phase locking the variations to the bunches. At present time resolved studies seem to be of interest in Biology [36,37].

It should be noted that with single or few bunch operation the beam current i is considerably less then the maximum value given in the data list of Fig. 6.

3.4 SR from wigglers and undulators

With a given storage ring, E_{cB} can be increased if an odd number, e.g. 3 to 11, of alternatively magnetized dipole magnets, a so-called 'wiggler', with a larger field B_W than the field B_B of the ordinary bending magnets is introduced into an otherwise straight section of the electron orbit (Fig. 7). SR from the wiggler has a higher E_{cW} according to [38]

$$E_{cW} = E_{cB}\frac{B_W}{B_B} \qquad (24)$$

The ratio B_W/B_B can be as large as 4 with superconducting magnets [39]. Wigglers are planed or in operation with 5 of the storage rings of Table 5. Besides shifting E_c the wiggler increases also the intensity by a factor which is roughly given by the number of radiating turns, i.e. 2 in Fig 7. At the same time the beam is widened which for certain applications may be disandvantageous.

Undulators are wiggler like magnet systems with a large number m of dipole units, where m is typically of the order of 100 (Fig. 8). The principal new effect occuring in the undulator is the coherent emission of SR by the individual electron from all turns simultaneously. The condition for coherence is that the time difference for an electron and the light at the distance λ_o of two wiggles is equal to the period of the light wave. The emitted spectrum is no longer continous but consists of a set of discrete wavelengths. The wavelength λ_i (i^{th} harmonic) which can be obtained at an angle θ from the trajectory is [26]

$$\lambda_i = \frac{1}{i}\frac{\lambda_o}{2\gamma^2}(1 + \gamma^2\vartheta^2 + \alpha^2\gamma^2/2) \qquad (25)$$

The fundamental is with E_e in GeV and λ_o in cm

$$\lambda_1 = 13\,\frac{\lambda_o}{E_e^2}\ [\text{Å}] \qquad (26)$$

α is the maximum deflection angle of the electron beam. The undulator provides a set of lines which are very strong because all the intensity of the previous continuum is concentrated in the lines. For the ESRF various undulators have been studied [26] . One example gives with 90 dipoles and

$$K \equiv \alpha\gamma = eB_o\lambda_o/(2\pi mc) = 0.9337\ B_o\lambda_o,\ B_o[\text{Tesla}]\lambda_o[\text{cm}] \qquad (27)$$

where B_o is the magnetic field and m the electron mass, for K = 2, λ_o = 5.6 cm a band ranging from 8.7 Å to about 0.46 Å (19^{th} harmonic). The total emitted power is about 6 kW and 3×10^{16} photons are emitted per sec at 1 Å at $\Delta\lambda/\lambda = 0.05$ in the 9^{th} harmonic. The whole set of lines can be shifted by changing the magnetic field B_o and hence the value of K. The brightness n is expected to be improved by three to four orders of magnitude compared with normal bending magnets.

A different type of undulator is based on the use of an helical magnetic field instead of an array of dipole fields [43,44,45].The helical undulator has properties similar to those of the plane undulator.

4. SUMMARY AND CONCLUSIONS

The main categories by which we have discussed the properties of the various kinds of X-ray sources were intensity N (or N'), brightness n and their dependence on direction and/or wavelength. Within the limitations of the approximations used we may summarize the results very roughly by comparing the data obtained for MoKα wavelength of all sources directly. For a more detailed comparison the reader is refered to the data given in Tables 1, 3, 4, and 5 or encouraged to calculated himself intensities from the expressions given as equations (4), (7) and (21).

sealed off X-ray tube	$N_B < 10^5$	$n_B < 2\times10^5$
	$N_L < 6\times10^7$	$n_L < 8.5\times10^7$
rotating anode tube	$N_B < 2.7\times10^6$	$n_B < 2.7\times10^6$
	$N_L < 1.2\times10^9$	$n_L < 1.2\times10^9$
storage ring (DORIS)	$N' < 8\times10^{12}$	$n' < 4\times10^{12}$ $(\sigma_x\sigma_y = 2\ mm^2)$

$N[ph.s^{-1}mrad^{-2}/0.1\%\Delta E/E]$, $n[ph.s^{-1}mrad^{-2}mm^{-2}/0.1\%\Delta E/E]$
With all X-ray tubes N_L is peaked at characteristic wavelengths, but not with respect to direction. N_B is neither peaked in direction nor in wavelength. With storage rings N' is strongly collimated but not peaked with respect to wavelength.

From the data given we conclude that at MoKα wavelength a SR source like DORIS gives about 6×10^3 photons more than the characteristic line generated with a rotating anode tube, provided the acceptance of the apparatus to be supplied

with photons is no more than about 1 $mrad^2$. With increasing σ'_z the photon number obtained with X-ray tubes increases correspondingly whereas with the SR source it remains constant for a fixed energy band. On the other hand, with a characteristic line the energy band is limited to about 3 to 5×10^{-4}. If the experiment can afford a wider band then with a SR source the intensity will increase whereas it will remain constant with a line source.

Another extremely important feature of the SR source is that, when combined with a suitable narrow band monochromator [46,47], it is in effect a tunable line source. In a similar way with bremsstrahlung also a tunable line source can be realized, however, as has been shown with the data of Tables 3,4 and 5, such a source has extremely low intensity when compared with the SR source.

Table 1 Intensity N_L of characterictic lines and intensity N_B of bremsstrahlung at the line energy E_{jz} for some typical target materials. E_{ejz} is the minimum excitation energy of the line. Tube voltage U = 40 kV, tube current i = 40 mA

Target material	z	Line	E_{ejz} [keV]	E_{jz} [keV]	$N_L \times 10^{-6}$ ($\delta=6^o$) [phot. s^{-1} $mrad^{-2}$ per 0.1% $\Delta E/E$]*	$N_B \times 10^{-3}$
Fe	26	Kα	7.10	6.40	99	36
Cu	29	"	8.86	8.05	77	39
Mo	42	"	20.0	17.5	13	39
Ag	47	"	25.5	22.2	4.5	35
Au	79	$L\alpha_1$	11.9	9.73	13	100

*for N_L $\Delta E/E$ is the natural width which is roughly (0.5 to 0.3) x 10^{-3}

Table 2. Experimental quantum efficiencies K_{jz} and absorption factor f (δ) for characteristic line production after Green [12] for typical lines and tube voltages U. z is the atomic number.

Line	z	$K_{jz} \times 10^6$ [$keV^{-1.63}$]	f (δ) 10	($\delta=6^o$) for 20	U [kV] = 30	40
CrKα	24	34				
FeKα	26	30	0.98			0.56
CoKα	27	27				
NiKα	28	25				
CuKα	29	22		0.86	0.75	0.65
MoKα	42	6.4				0.78
AgKα	47	4.0			0.84	0.73
WKα	74	0.31				
AuKα	79	0.19				
$AuL\alpha_1$	79	7.0		0.70	0.54	0.42

Table 3. Characteristics of sealed off X-ray tubes with Mo target. N_L, N_B are intensities for Kα radiation and bremsstrahlung at the Kα wavelength calculated with equations (7) and (4), respectively.

Typ		F 60 - 01	F 60 - 04	F 60 - 10	F 60 - 20	FA 100
Focus l	[mm]	8	8	10	12	
w	[mm]	0.15	0.4	1	2	
Max. load P_m	[kW]	0.8	2.0	2.4	2.7	3.0
U_{max}	[kV]	60	60	60	60	100
i at P_m	[mA]	13	33	40	45	30
source size ($\delta=(6^o)$	[mm^2]	0.12	0.32	1	2.4	
max. specific load p_m	[kW mm^{-2}]	0.67	0.63	0.24	0.11	
$N_L x10^{-6}$	[ph.s^{-1}mrad^{-2} per 0.1% ΔE/E]	10	3 3	3 2	3 5	6 1
$N_B x10^{-3}$	"	23	59	71	80	104
$n_L x10^{-6}$	[ph.s^{-1}mrad^{-2} mm^{-2} per 0.1% ΔE/E]	8 5	7 9	3 2	1 5	
$n_B x10^{-3}$	"	192	184	71	33	

Table 4. Characteristics of rotating anode tubes with Mo target. N_L, N_B are intensities for Kα radiation and bremsstrahlung at the Kα wavelength calculated with equations (7) and (4), respectively

Typ		RU 200	RU 200	RU 500	RU 1000	RU 1500	GX - 6
Focus l	[mm]	10	3	10	10	10	3
w	[mm]	0.5	0.3	0.5	1	1	0.3
Max. load P_m	[kW]	12	5.4	30	60	90	4.0
U_{max}	[kV]	60	60	60	60	60	50
i at P_m	[mA]	200	90	500	1000	1500	80
source size ($\delta=6^o$)	[mm^2]	0.5	0.09	0.5	1	1	0.09
max. specific load p_m	[kWmm^{-2}]	2.4	6	6	6	9	4.4
$N_L x10^{-6}$	[ph.s^{-1}mrad^{-2} per 0.1%ΔE/E]	150	70	390	780	1170	40
N_B x 10^{-3}	"	357	160	892	1784	2676	109
$n_L x10^{-6}$	[ph.s^{-1}mrad^{-2} mm^{-2}per 0.1%ΔE/E]	300	780	780	780	1170	440
n_B x 10^{-3}	"	714	1778	1784	1784	2676	1211

Table 5. Storage rings suited for X-ray generation
Comparison of intensities N'

Name	Location	Remarks*	E_c [keV]	λ_c [Å]	σ'_z at E-10keV [μrad]	$N'[10^{11}$ ph.s^{-1}mrad^{-1}perO.1%ΔE/E] at E [keV] = (FeKα) 6.42	(CuKα) 8.06	(MoKα) 17.52	(AgKα) 22.21
SRS	Daresbury, UK	dedicated, under construction, also wiggler	3.2	3.88	83	130	95	6.6	1.9
DCI	Orsay, France	SR Lab	3.39	3.67	96	58	39	3.3	0.98
Photon Factory	Tsukuba, Japan	dedicated, under constr.	4.18	2.97	76	134	97	14	4.4
NSLS	Upton,NY.USA	" wiggler	5.0	2.48	83	163	127	26	12
VEPP-3	Novosibirsk,USSR	SR Lab. wiggler	5.6	2.22	88	36	29	7.2	3.5
SPEAR	Stanford,Cal.USA	2 SR Labs wiggler	11.2	1.1	76	50	46	25	18
ESRF	Europe	study,also undulator	12.4	1.0	63	599	562	335	248
VEPP-4	Novosibirsk,USSR	under constr. SR Labs	14.5	0.86	57	131	123	83	65
DORIS	Hamburg,F.R.G.	2 SR Labs	23	0.54	82	113	112	93	81
CESR	Ithaca,NY.,USA	under constr. SR Labs	35	0.36	68	176	180	171	160
PEP	Stanford,Cal.,USA	under constr.	45.4	0.27	53	320	329	333	321
PETRA	Hamburg,F.R.G.	no SR Lab	77.2	0.16	57	331	346	383	385

*The operating parameters E_0 [GeV], R [m] and i [mA] are given in Fig. 6

References

1. R. Wideröe (1951) Brown Boveri Mitt. 38, 260
2. K. Gund (1953) Stahl u. Eisen 73, 710
3. H. Kulenkampff (1922) Ann. Phys. 69, 548
4. H. Kulenkampff (1926) Handbuch der Physik, edited by Geiger and Scheel, Vol. 23, pp. 433
5. H. Kulenkampff & L. Schmidt (1943) Ann. Phys. (5) 43, 494
6. P. Kirkpatrik (1927) Phys. Rev. 22, 226
7. E. Wagner & P. Ott (1928) Ann. Phys. 85, 425
8. W.W. Loebe (1914) Ann. Phys. 44, 1033
9. M. Green (1963) in X-ray Optics and Microanalysis, (ed. H.H. Pattee, V.E. Cosslett & A. Engström) Academic Press, New York and London, p. 185
10. M. Green & V.E. Cosslett (1961) Proc. Phys. Soc. (London) 73, 924
11. J.A. Bearden (1974) in International Tables for x-ray Crystallography Vol. IV (ed. J.A. Ibers & W.C. Hamilton), The Kynoch Press, Birmingham, p. 20
12. M. Green (1963) in X-Ray Optics and Microanalysis, (ed. H.H. Pattee, V.E. Cosslett & A. Engström) Academic Press, New York and London, p. 361
13. A.E. Sandström (1957) in Handbuch der Physik Vol. 30, edited by S. Flügge, Springer Verlag Berlin, Göttingen, Heidelberg, pp. 78
14. W. Rump (1927) Z. Physik 43, 254
15. H.A. Kramers (1923) Phil. Mag. 46, 836
16. M. Yoshimatsu & S. Kozaki (1977) in X-Ray Optics, Topics in Applied Physics Vo. 22 (ed. H.-J. Queisser) Springer Verlag Berlin, Heidelberg New York, p. 7

17. J. Schwinger (1949) Phys. Rev. 75, 798

18. T. Tuomi, K. Naukkarinen, E. Laurika & P. Rabe (1973) Acta polytech. Scand. Ph100, 1

19. T. Tuomi, K. Naukkarinen & P. Rabe (1974), phys. stat. sol. (a) 25, 93

20. M. Hart (1975) J. Appl. Cryst. 8, 436

21. U. Bonse & G. Materlik (1975) in Anomalous Scattering (ed. by S. Ramaseshan & S.C. Abrahams) Mungsgaard Kopenhagen, p. 107

22. P. Eisenberger & B.M. Kincaid (1975) Chem. Phys. Lett. 36, 134

23. J. Barrington Leigh & C. Rosenbaum (1974) J. Appl. Crystallogr. 7, 117

24. L. Lindau, P. Pianetta, K.Y. Yu & W.W. Spicer (1976) Phys. Rev. B13, 492

25. W. Gudat & C. Kunz (1979) in Synchroton Radiation, Techniques and Applications (ed. by C. Kunz), Topics in Current Physics, Vol.10, Springer Verlag Berlin, Heidelberg, New York, p.55

26. Y. Farge (ed.) (1979) Feasibility Study for a European Synchrotron Radiation Facility, European Sciene Foundation, Straßburg

27. J.R. Stevenson, H. Ellis & R. Bartlett (1973) Applied Optics 12, 2884

28. D. Einfeld & D. Stuck (1976) Opt. Comm. 19, 197

29. E. Pitz (1969) Appl. Opt. 8, 255

30. R. Haensel & C. Kunz (1967) Z. angew. Phys. 23, 276

31. R. Godwin (1969) in Springer Tracts in Modern Physics Vol.51 (ed. by G. Höhler) Springer Verlag Berlin, Heidelberg, New York

32. C. Kunz (ed). (1979) Synchrotron Radiation, Techniques and Applications, Topics in Current Physics Vol. 10, Springer Verlag Berlin, Heidelberg, New York

33. J. Schwinger (1949) Phys. Rev. 75, 1912

34. D.H. Tomboulian & P.L. Hartmann (1956) Phys. Rev. 102, 1423

35. J.D. Jackson (1975) Classical Electrodynamics, John Wiley, New York London Sydney Toronto, p. 676

36. H.B. Stuhrmann (1978) Quarterly Review of Biophysics II,I, 71

37. J. Barrington Leigh & C. Rosenbaum (1976) Ann. Rev. Biophysics and Bioengeneering 5, 239

38. H. Winik & R. Hehn (1978) Nucl. Instr. Meth. 152, 9

39. D.E. Baynham, P.T.M. Clee & D.J. Thompson (1978) Nucl. Inst. Meth. 152, 31

40. H. Motz (1951) J. Appl. Phys. 22, 527

41. D.F. Alferov, Yu. A. Bashmakov & E.G. Bessonov (1976) in Synchrotron radiation, Lebedev Phys. Inst. Series 80 (ed. N. G. Basov) New York Consultants Bureau, p 97

42. A. Hofmann (1978) Nucl. Instr. Meth. 152, 17

43. D. F. Alferov, Yu. A. Bashmakov & E.G. Bessonov (1974) Sov. Phys. Tech. Phys. 18, 1336

44. L. R. Elias et al. (1976) Phys. Rev. Lett. 36, 717

45. B.M. Kincaid (1977) J. Appl. Phys. 48, 2684

46. J. A. Beaumont & M. Hart (1974) J. Phys. (E) 7, 823

47. U. Bonse, G. Materlik & W. Schröder (1976) J. Appl. Cryst.9,223

Figure Captions

Fig. 1 Geometry used for defining source characteristics. X-ray source extending in X,Z plane. The direction of emission is given by angles ψ and ξ. σ_x, σ_z source dimensions in X- and Z- directions, respectively.

Fig. 2 Conventional sealed off X-ray tube with stationary anode and water cooling. The Wehnelt cylinder may be used for focusing the electron beam on the anode. The X-ray beam is taken off at an angle δ against the anode surface. The size of the actual source S may be varied by altering δ and also by taking the beam off along the X-direction resulting in a line source.

Fig. 3 Permanently pumped rotating anode tube with water cooled anode.

Fig. 4 Geometry of a storage ring source. For a given tangent point at the orbit the radiation is contained within a cone of opening σ_z' which narrows with E_e and E. The effective source size $\sigma_z \times \sigma_x$ is determined jointly by the crossectional size of the electron beam and the divergence σ_x' in the orbital plane accepted by the measuring apparatus.

Fig. 5 Dependence of Polarization of SR on the angle ψ against the electron orbit. Note that shorter wavelengths are more collimated near $\psi = 0$.

Fig. 6 Calculated intensities N' for the twelve storage rings listed in Table 5. E_e is electron energy, R magnetic radius of orbit and i the electron current.

Fig. 7 Wiggler with five dipole magnets.

Fig. 8 Principle of an undulator with a large number (typically 100) of dipoles for coherent emission of SR for any individual electron.

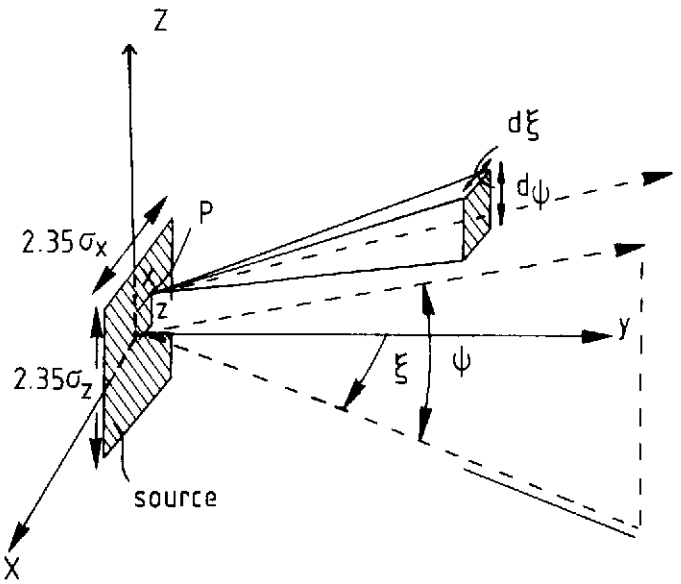

Fig. 1 Geometry used for defining source characteristics. X-ray source extending in X,Z plane. The direction of emission is given by angles ψ and ξ. σ_x, σ_z source dimensions in X- and Z- directions, respectively.

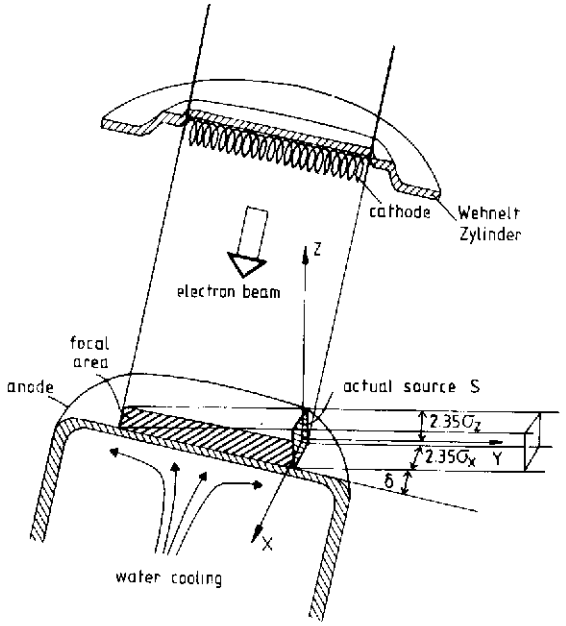

Fig. 2 Conventional sealed off X-ray tube with stationary anode and water cooling. The Wehnelt cylinder may be used for focusing the electron beam on the anode. The X-ray beam is taken off at an angle δ against the anode surface. The size of the actual source S may be varied by altering δ and also by taking the beam off along the X-direction resulting in a line source.

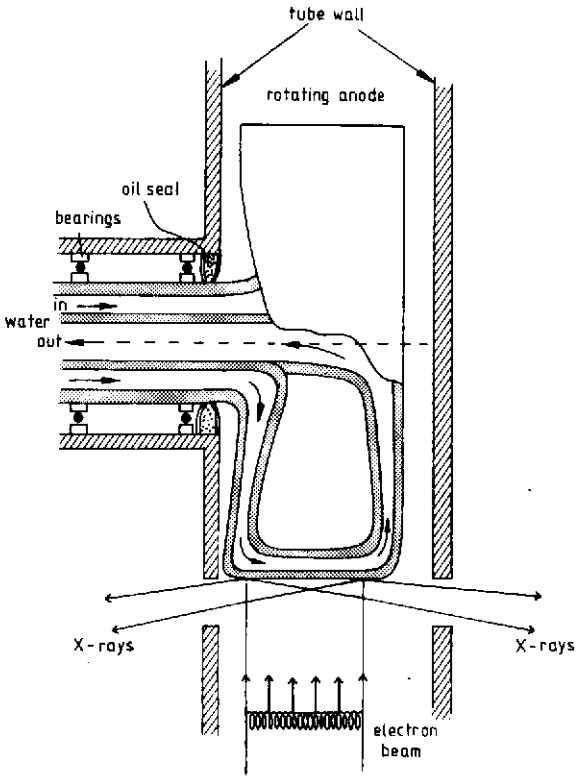

Fig. 3 Permanently pumped rotating anode tube with water cooled anode.

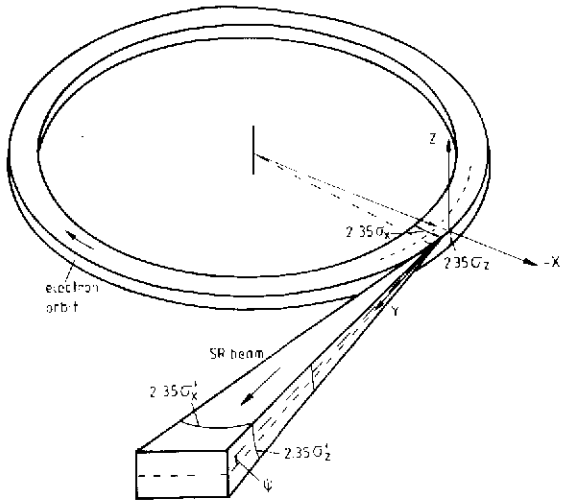

Fig. 4 Geometry of a storage ring source. For a given tangent point at the orbit the radiation is contained within a cone of opening σ'_z which narrows with E_e and E. The effective source size $\sigma_z \times \sigma_x$ is determined jointly by the crossectional size of the electron beam and the divergence σ'_x in the orbital plane accepted by the measuring apparatus.

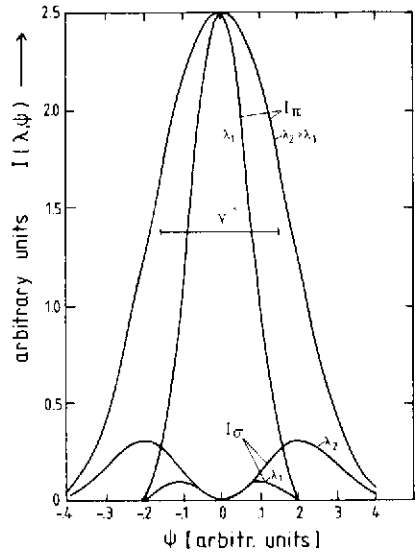

Fig. 5 Dependence of Polarization of SR on the angle ψ against the electron orbit. Note that shorter wavelengths are more collimated near ψ = 0.

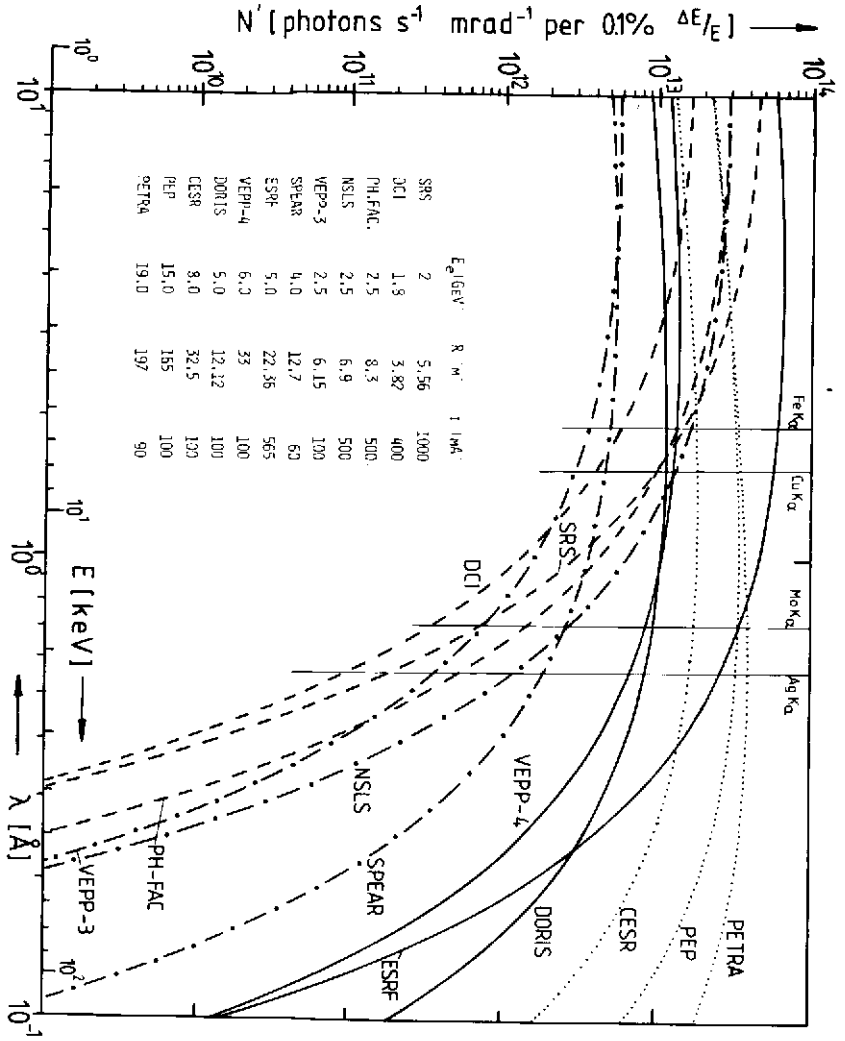

Fig. 6 Calculated intensities N' for the twelve storage rings listed in Table 5. E_e is electron energy, R magnetic radius of orbit and i the electron current.

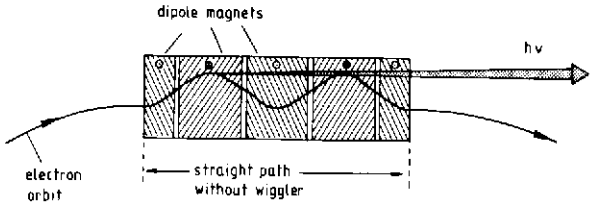

Fig. 7 Wiggler with five dipole magnets.

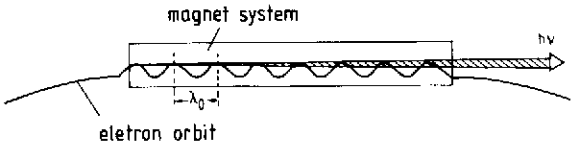

Fig. 8 Principle of an undulator with a large number (typically 100) of dipoles for coherent emission of SR for any individual electron.